GFZ POTSDAM

VNIVERSITAT DE VALÈNCIA

Algorithm Theoretical Basis Document

CHRIS/PROBA
Atmospheric Correction Module

Version 2.0, May 20, 2008

Luis Guanter[1], Luis Alonso[2], Luis Gómez-Chova[2], Jose Moreno[2]

[1] *GeoForschungsZentrum Potsdam, Telegrafenberg 14473, Potsdam (Germany)*

[2] *University of Valencia, Dr. Moliner 50, 46100, Burjassot–Valencia (Spain)*

Development of CHRIS/PROBA modules for the BEAM toolbox
ESA ESRIN Contract No. 20442/07/I-LG

Contents

Abstract

The so-called atmospheric correction, i.e. the conversion from Top-of-Atmosphere radiance to reflectance images, is normally necessary for the relieble exploitation of remote sensing information. The theoretical basis of the atmospheric correction algorithm for Compact High Resolution Imaging Spectrometer (CHRIS) on board the PRoject for On-Board Autonomy (PROBA) to be implemented in the Basic ERS & Envisat (A)ATSR and MERIS (BEAM) software is described in this document. Atmospheric correction should be performed on the outputs from the noise reduction and cloud screening modules also implemented in BEAM. The atmospheric correction module can process data from the 5 different CHRIS acquisition modes, which define the spectral and spatial specifications of the data. Depending on the acquisition mode, assessment of spectral calibration, retrieval of aerosol optical thickness and columnar water vapor, and radiometric recalibration are carried out along the complete processing. The validation exercise consisting in the comparison of CHRIS/PROBA-derived data with ground-based measurements performed during the development phase is also presented in this document. Special effort has been put on the validation of the atmospheric parameters retrieved from CHRIS/PROBA by comparison with data from the AErosol RObotic NETwork (AERONET).

Acronyms and Abbreviations

AERONET AErosol RObotic NETwork

AOT Aerosol Optical Thickness

ASD Analytical Spectral Devices FieldSpec Pro FR Spectroradiometer

ATBD Algorithm Theoretical Basis Document

BEAM Basic ERS & Envisat (A)ATSR and MERIS

BRDF Bidirectional Reflectance Distribution Function

CHRIS Compact High Resolution Imaging Spectrometer

CWV Columnar Water Vapor

DEM Digital Elevation Model

ELEV ELEVation

FZA Fly-by Zenith Angle

LUT Look-Up Table

MODTRAN MODerate resolution TRANsmittance

NDVI Normalized Difference Vegetation Index

NIR Near–infraRed

PROBA PRoject for On-Board Autonomy

RAA Relative Azimuth Angle

SPARC SPectra bARrax Campaign

SZA Sun Zenith Angle

TOA Top Of Atmosphere

VZA View Zenith Angle

1 Introduction

1.1 Purpose

This Algorithm Theoretical Basis Document (ATBD) describes an algorithm for the atmospheric correction of data acquired by the Compact High Resolution Imaging Spectrometer (CHRIS) on board the Project for On-Board Autonomy (PROBA) platform (Barnsley et al., 2004). The algorithm is to be implemented in the Basic ERS & Envisat (A)ATSR and MERIS (BEAM) software (Fomferra and Brockmann, 2005), together with other packages for the processing and exploitation of CHRIS/PROBA data. This atmospheric correction module will convert from Top-of-Atmosphere (TOA) radiance to surface reflectance images in an automatic manner. The different steps to be performed along the atmospheric correction process depend on the CHRIS acquisition mode. The aerosol optical thickness (AOT) characterising the atmospheric aerosol loading is calculated for all the CHRIS acquisition modes, while columnar water vapor (CWV) is only derived for modes 1, 3 and 5, as no sufficient sampling of water vapor absorption features is provided by modes 2 and 4. On the other hand, spectral calibration and an optional spectral polishing are only performed on modes 1 and 5, which are the ones resolving most of the atmospheric absorption bands in the 400-1000 nm spectral range. The algorithm is implemented so that it must be applied after noise removal and cloud screening. The interface between atmospheric and geometric correction modules is not established at this stage of this project, so elevation and topographic effects calculated from a geo-located digital elevation model are not considered in current version of the atmospheric correction module. This document outlines the algorithm physical and mathematical basis, and lists the assumptions and limitations of the proposed algorithm.

1.2 CHRIS/PROBA data

The CHRIS/PROBA system (Barnsley et al., 2004), launched on 22 October 2001, was implemented as a technology demonstration experiment to take advantage of autonomous pointing capabilities of a generic platform suitable for Earth Observation purposes. It provides high spatial resolution hyperspectral and multiangular data, what constitutes a new generation of remote sensing information to be processed and exploited.

On one hand, the PROBA platform provides pointing in both across–track and along–track directions. In this way, the CHRIS/PROBA system has multiangular capabilities, acquiring up to 5 consecutive images from 5 different view angles in the same satellite overpass. Each imaged target has an associated "fly–by" position, that is the position on the ground track when the platform zenith angle, as seen from the target, is a minimum. The platform acquires the images at times when the zenith angle of the platform with respect to the fly–by position is equal to a set of Fly–by Zenith Angles (FZA): 0°, ±36° or ±55°. Negative FZAs correspond to acquisition geometries for which the satellite has already flown over the target position.

On the other hand, CHRIS measures over the visible and near–infrared (NIR) bands from

410 nm to 1050 nm, with the internal spectral resolution ranging between 1.25 (@400 nm) and 11 nm (@1000 nm). The spectral configuration is set in advance through the selection of one of 5 possible acquisition modes, which define combinations of number, position and width of spectral channels, as well as spatial resolution and coverage. For each of those acquisition modes, bands spectral position are expected to change from one acquisition to another due to thermal variations in the instrument. The spectral coverage of bands acquired by the different CHRIS modes is depicted in Fig. 1.

Apart from the particular band setting, acquisition modes also define the ground sampling distance (GSD) and the swath width. Nominal GSD is 34 m for mode 1, and 18 m for the rest of the modes, while the nominal swath width is about 13 km for all the modes except for mode 5, which operates with half-swath.

1.3 On the atmospheric correction of hyperspectral data

Airborne or spaceborne imaging spectrometers allow the remote monitoring of surface and atmospheric processes. In particular, a wide range of scientific fields, such as mineral mapping, vegetation phenology, water quality or atmospheric chemistry, can be covered by instruments with a fine spectral resolution. When the acquired remote sensing data set is to be used in the characterisation of the surface state, the target reflectance becomes the natural magnitude to be evaluated. The atmospheric contribution to the radiance spectra measured by the sensor becomes an error source that must be removed from the useful signal reflected by the surface, which is the principle of atmospheric correction.

Advanced atmospheric correction algorithms for hyperspectral data lie on a radiative transfer approach to invert the surface reflectance from the at-sensor radiance registered by the sensor. The atmospheric components with the highest optical activity in the solar spectrum range are aerosols and water vapor. The general situation is that no ancillary information about particulate matter or water vapor abundances simultaneous to image acquisitions is available except for some dedicated field experiments. For these reason, algorithms for the estimation of AOT or CWV from the hyperspectral data themselves must be coupled to atmospheric radiative transfer codes to simulate the atmospheric interaction with the solar radiation traveling across it.

However, apart from the atmosphere there are other error sources affecting the retrieved surface reflectance. One of the most important ones is the deviation of spectral channels position and width from nominal values. Optical aberrations in pushbroom systems, such as CHRIS, may cause the spectrometer entrance slit to be projected as a curve on the rectilinear detector array (Mouroulis et al., 2000; Qu et al., 2003). This originates a combination of bending of spectral lines across the spatial axis and of the spatial lines across the spectral axis. The first effect, known as “smile”, originates a non-linear variation of the spectral shift with the across-track position of the different detectors compounding the sensor. Degradation in the instrument calibration can also lead to a wrong spectral response. Spectral shifts from the band positions defined at the laboratory and provided to the users lead to noticeable errors in surface reflectance, especially in

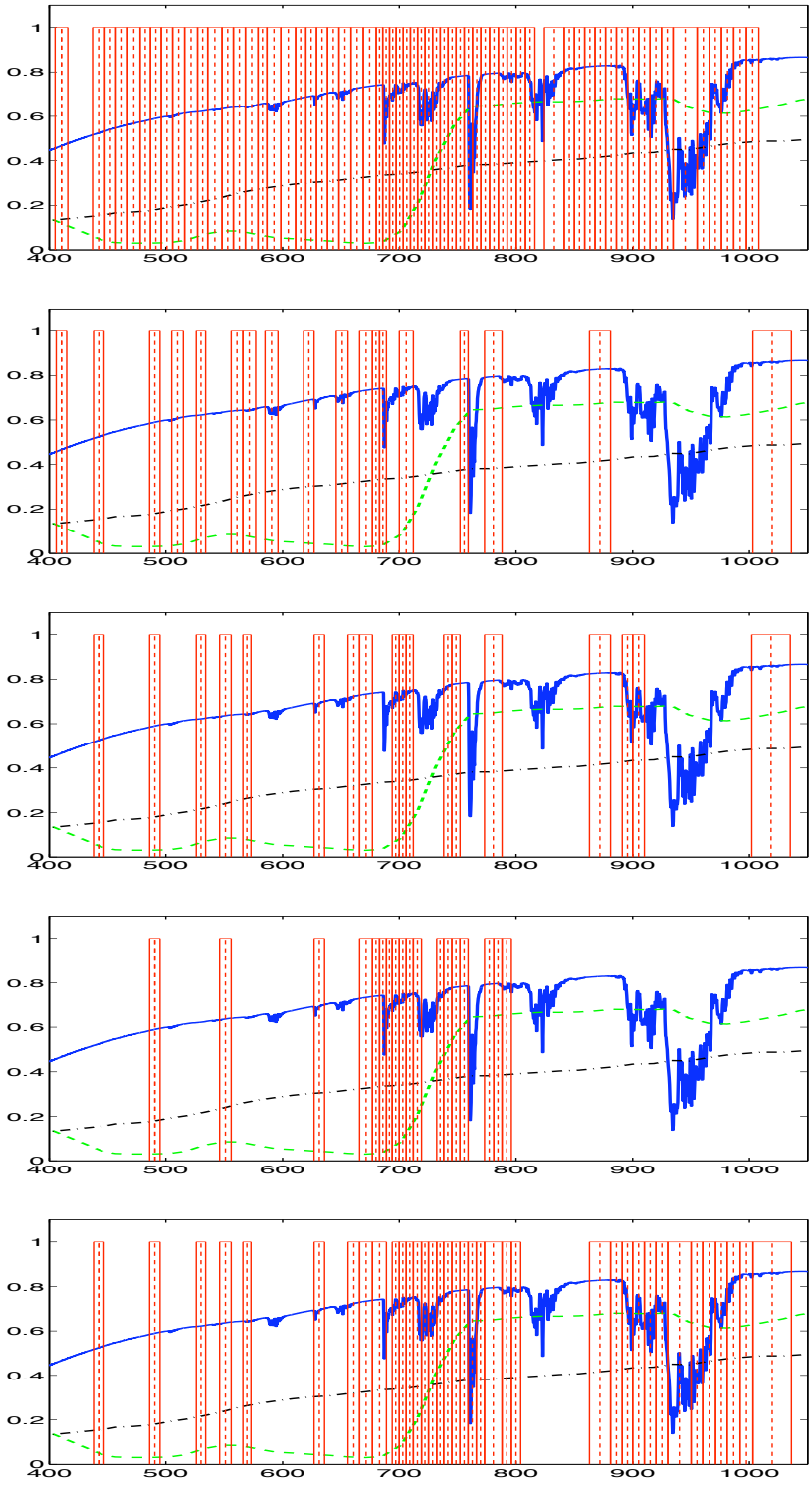

Figure 1: *Top-to-bottom*: CHRIS modes 1–5 band locations (boxes) superimposed to a reflectance spectra of healthy vegetation (dashed), bare soil (dash-dotted), and the atmospheric transmittance (solid). Vertical axis is in normalised units and the horizontal axis is in nanometers (reproduced from Gómez-Chova et al. (2008b)).

those bands located in the surroundings of gaseous absorptions. A detailed analysis of the errors in at-sensor radiances caused by systematic shifts was presented by Green (1998). Synthetic data with a systematic spectral shift of 1 nm for channels with Full Width at Half Maximum (FWHM) of 10 nm showed associated errors in the measured radiance of up to ±25% in strong water vapor absorption bands. In addition, instrumental noise or errors in calibration coefficients or atmospheric characterisation may cause errors in the retrieved reflectance to appear all over the spectral range.

The influence of both atmospheric and instrumental factors over the retrieval of surface reflectance is addressed in the proposed algorithm. However, the complete processing chain is conditioned by the CHRIS acquisition mode. Good spectral resolution and sampling are necessary for water vapor retrieval and the assessment of the spectral calibration, as those are achieved by means of the resolution of atmospheric absorption features. For the same reason, errors in reflectance associated to a bad characterisation of CWV or sensor calibration are minimised for coarser spectral resolutions or when atmospheric absorption features are skipped. In the case of CHRIS acquisition modes, the entire 400-1000 nm spectral range is only registered by mode 1, as it is shown in Fig. 1. Atmospheric oxygen A and B bands, at 687 and 760 nm respectively, are only registered in modes 1 and 5, and the strong water vapor absorption feature centered at 940 nm is totally or partially covered in modes 1, 3 and 5. For this reason, CWV retrieval is not carried out in modes 2 and 4, and the assessment of sensor calibration is only performed on modes 1 and 5. AOT retrieval is performed for all the acquisition modes, as it is mostly driven by aerosol scattering, which presents a continuous spectral dependence.

1.4 Document outline

A full description of the algorithm is presented in this document. Two sections follow this introduction. The first one deals with the description of the algorithm physical basis, covering the different processing steps leading to the final reflectance product. Some notes about the algorithm performance and general input and output parameters are also provided. A second section presents results about previous validation of the algorithm over both land and water targets. It must be remarked that some of the assumptions and steps described hereinafter apply only to modes 1 and 5, the other three modes being considered particular cases.

2 Algorithm Description

2.1 Theoretical description

2.1.1 Radiative transfer calculations and LUT

The retrieval of atmospheric constituents and surface reflectance involves modeling the radiative transfer across the atmosphere. A simple but accurate formulation of the TOA signal in terms of surface reflectance and atmospheric optical parameters is necessary. Since no knowledge of the

surface bidirectional reflectance distribution factor (BRDF) is available prior to the atmospheric correction, the usual Lambertian approach (Nicodemus et al., 1977) for the surface reflectance is assumed. This leads to the well–known equation

$$L_{\mathrm{TOA}} = L_0 + \frac{1}{\pi}\frac{\rho_s(E_{\mathrm{dir}}\mu_{\mathrm{il}} + E_{\mathrm{dif}})T_{\uparrow}}{1 - S\rho_s} \tag{2.1}$$

where L_{TOA} is the TOA radiance, L_0 is the atmospheric path radiance; μ_{il} is the cosine of the illumination zenith angle, measured between the solar ray and the surface normal; $E_{\mathrm{dir}}\mu_{\mathrm{il}}$ and E_{dif} are the direct and diffuse fluxes arriving at the surface, respectively; S is the atmospheric spherical albedo, reflectance of the atmosphere for isotropic light entering it from the surface; $T_{\uparrow}$ is the total atmospheric transmittance (for diffuse plus direct radiation) in the observation direction, and ρ_s is the surface reflectance.

The MODerate resolution TRANsmittance (MODTRAN4) atmospheric radiative transfer code (Berk et al., 2003) was used for the generation of a Look-Up Table (LUT) which provides the atmospheric parameters from multidimensional linear interpolation. MODTRAN4 has been selected for its good parameterisation of both scattering and absorption atmospheric processes, as interposed by an algorithm dealing with simultaneous aerosol and water vapor retrieval. The LUT depends on 6 free input parameters: view zenith angle (VZA), solar zenith angle (SZA), relative azimuth angle (RAA), surface elevation (ELEV), aerosol optical thickness at 550 nm (AOT550) and columnar water vapor (CWV). The original MODTRAN4 code was modified so that the atmospheric optical parameters needed for the atmospheric correction in Eq. 2.1 were provided as output, as they are not in the original MODTRAN4 code. The atmospheric vertical profile is given by the default midlatitude summer atmosphere, the aerosol type is fixed to the continental model, and the ozone concentration is fixed to 7.08 g·m^{-2}.

The optimum breakpoint positions for the 6 input parameters are presented in Table 1. The number of breakpoints describing each dimension in the LUT was selected as a tradeoff between sufficient sampling and LUT size. For this purpose, radiative transfer simulations provided the dependencies of physical magnitudes on the 6 free parameters. A number from 3 to 7 provided a sufficient sampling of the parameter space without leading to unaffordable computation times or LUT size. For the selection of the breakpoint positions, their influence on scattering and absorption processes was analysed. Atmospheric path radiance at a blue wavelength (410 nm) was selected to describe scattering, while the ratio between pairs of absorption/reference bands described absorption. Breakpoints positions were selected so that the maximum parameter variation rates were properly sampled. The design and generation of this LUT is further desbribed in Guanter et al. (2008).

The use of the LUT for the calculation of atmospheric optical parameters enables to speed-up radiative transfer calculations, which is fully necessary if pixel-to-pixel variations caused by changes in surface elevation or water vapor are to be considered. The atmospheric parameters stored in the LUT cover the 400-1100 nm range with 1 nm spectral resolution, in order to enable the resampling to the particular spectral setting of each acquisition mode.

Table 1: Breakpoint positions in the LUT for the 6 input variables.

	#1	#2	#3	#4	#5	#6	#7	#8
VZA (°)	0	10	20	30	40	48	55	60
SZA (°)	0	10	20	35	50	60	70	–
RAA (°)	0	25	50	85	120	155	180	–
ELEV (km)	0	0.7	1.5	2.5	–	–	–	–
AOT@550 ()	0.05	0.12	0.2	0.3	0.4	0.6	–	–
CWV ($g \cdot cm^{-2}$)	0.3	1	1.5	2	2.7	3.5	5	–

2.1.2 Spectral calibration

Different causes may originate the sensor spectral degradation, leading to spectral shifts from the nominal band positions. In addition, the so-called smile effect, describing the non-linear variation of channels spectral position in the acquisition across-track direction, is intrinsic to pushbroom instruments such as CHRIS. The first step in the atmospheric correction algorithm for modes 1 and 5 is the evaluation of potential problems in the instrument spectral calibration. Since a full description of the module characterising the spectral calibration is already reported in Guanter et al. (2006), only an overview is given here. As it has been already remarked, the spectral resolution provided by CHRIS modes other than modes 1 and 5 is not enough for a reliable spectral calibration, so this module would not be applied to them. However, the spectral calibration would not be a critical issue in the other modes for the same lack of spectral resolution.

Errors in surface reflectance appear around atmospheric absorption features when the band configuration applied in the resampling of the atmospheric parameters differs from the actual one. The fundamental basis for the detection of spectral shifts is the removal of those errors. The method looks for the shift which generates the smoothest surface reflectance spectrum after the atmospheric correction. The O_2 absorption feature centered at 760 nm is used as reference for the CHRIS spectral calibration. The across-track direction is represented by a set of radiance spectra derived by averaging all the spectra in the along-track direction into one single pixel for each image column. The spectral shift is evaluated independently for each one of them.

The characterisation of the smile effect in CHRIS for 2003 (old processing software) and 2005 (new processing software) spectral calibrations are presented in Fig. 2. Even though CHRIS is a pushbroom instrument, the design of the instrument was intended to avoid the smile effect. The successful performance of that design across the 385 pixels in the across–track direction can be checked. The change in the spectral shift is around 0.2 nm between the edges of the spectrometer. It must be remarked that the small change in the performance around pixel 230 is probably caused by a small defect in the slit. Those results compare well with an equivalent analysis performed by CHRIS' operators using an image acquired over open water during earlier stages of the CHRIS/PROBA mission (M. Cutter, Surrey Satellite Technology Ltd, personal communication, 2006). In view of these results, and in order to speed-up the processing, atmospheric correction

is not performed pixel-wise for the accurate consideration of smile, but only a mean value characterising the overall spectral shift from the nominal channel positions is used to update the later ones.

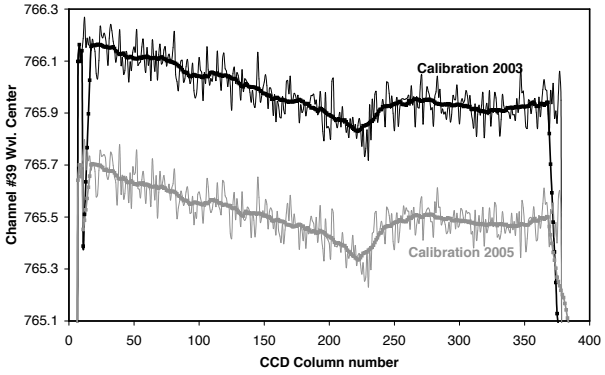

Figure 2: Characterisation of CHRIS spectral calibration from 2003 and 2005 data.

2.1.3 Retrieval of aerosol optical thickness

For the AOT retrieval over land targets, the technique already described in Guanter et al. (2005) is applied here. The total aerosol loading is parameterised by the AOT at 550 nm. No attempt to derive information on the aerosol model is made, but it is assumed that the aerosol optical properties are sufficiently described by the rural aerosol model implemented in MODTRAN4. It is also assumed that the AOT is constant all over the imaged area, which is about 13×13 km^2 side for those acquisition modes registering the entire swath.

The first step is masking out all the pixels affected by clouds. Making use of the probabilistic cloud mask provided by the cloud screening module (Gómez-Chova et al., 2008b), those pixels which are sure to be cloudy are removed. AOT550 is calculated as long as the scene contains more than 35% of cloud-free pixels. If the percentage of cloud-free pixels is lower than 35% it is assumed that the image is too contaminated by clouds for a reliable aerosol retrieval.

After cloud screening, the lowest radiance value in each spectral band within the image is found. The resulting spectrum is employed as a reference dark target. It provides the highest limit for the aerosol content: an iterative procedure looks for the AOT550 value leading to the atmospheric path radiance which is closest to the radiance in the dark spectrum, not allowing path radiance to be higher than the dark spectrum in any of the visible bands (from 410 to 680 nm). The lowest the radiance in the dark spectrum is, the closest the estimated AOT550 value will be to the real value. If no spectrum with relatively dark values is found, the retrieved aerosol loading will overestimate the real conditions. To avoid this situation, a lowest limit of AOT at 550 nm about 0.2 is arbitrarily chosen for this procedure: if the AOT550 value estimated as lowest limit is higher than 0.2, the dark pixel estimation is discarded.

The next step is refining that initial AOT550 estimation with a more sophisticated method

involving the inversion of TOA radiances in combinations of green vegetation and bare soil pixels. This is performed only over those pixels which are classified as land pixels. AOT550 is then retrieved from 5 pixels with high spectral contrast inside this window, by means of a multiparameter inversion of the TOA spectral radiances in those pixels. To provide an estimation of the surface reflectance, each of the 5 reference pixels is represented by a linear combination of two vegetation and soil spectra, which act as endmembers:

$$\rho_s = C_v \rho_{\mathtt{veg}} + C_s \rho_{\mathtt{soil}} \qquad C_{v,s} > 0,\ \rho_s \in [0,1] \tag{2.2}$$

where $\rho_{\mathtt{veg}}$, $\rho_{\mathtt{soil}}$ are representative vegetation and bare soil reflectance spectra, and $C_{v,s}$ the weighting coefficients. The proportions of vegetation and soil are allowed to be larger than 1.0, covering those cases in which the surface reflectance is brighter than the endmembers. The constraint is that the generated surface reflectance must be in the range $[0, 1]$. The ten abundance coefficients $C_{v,s}$ (2 for each of the 5 pixels) are free parameters in the inversion, as well as the aerosol loading. The resulting 11-D inversion is performed by the Powell Minimization Method (Press et al., 1986). It must be remarked that the vegetation and bare soil endmembers are not real endmembers characterising every single scene, but they are only used to represent the average surface reflectance contribution by means of its linear combination. Thus, there is no need for the retrieval of endmembers from the image, but it is enough if the a priori selected spectra can be combined to reproduce the actual spectral shape of the reference pixels. A similar idea using linear combinations of endmembers to be inverted inside an AOT retrieval scheme was proposed by von Hoyningen-Huene et al. (2003).

The 5 reference pixels must have as much spectral contrast as possible (ranging from pixels with high vegetation content to high bare soil content). The reason is that this contrast in the surface, while assuming a constant atmosphere above, is used in the discrimination of the radiative transfer contribution of surface and atmosphere to the TOA signal. In order to minimise possible biases due to a bad representation of the actual surface reflectance by endmember combinations, three different vegetation spectra are combined with one bare soil spectrum to simulate each reference pixel. Those three vegetation spectra, plotted in Fig. 3, correspond to a green vegetation crop, a typical forest spectrum and a dark vegetation target. The aerosol loading is calculated independently for each of the three pairs of vegetation and soil endmembers. The AOT value leading to the minimum value of the merit function driving the inversion is selected for the image. The reason for having 3 vegetation spectra accounting for different vegetation types and only one for bare soil is that vegetation is considered to have a wider range of spectral patterns than bare soils.

In the case of inland water pixels, the particular performance of CHRIS in the mode 2 configuration (optimised for the observation of water bodies) causes that a different approach must be followed in the retrieval of the atmospheric parameters. The use of land pixels is avoided for mode 2 data, due to the saturation usually found for surface albedoes higher than 20-25%. An iterative procedure is again performed for aerosol retrieval over water pixels. It seeks for the AOT550 that minimises the subsequent water reflectance in CHRIS bands 2 and 3 (centered around 440 and 490 nm in mode 2), where the aerosol scattering is maximal, with the physical constraint that the

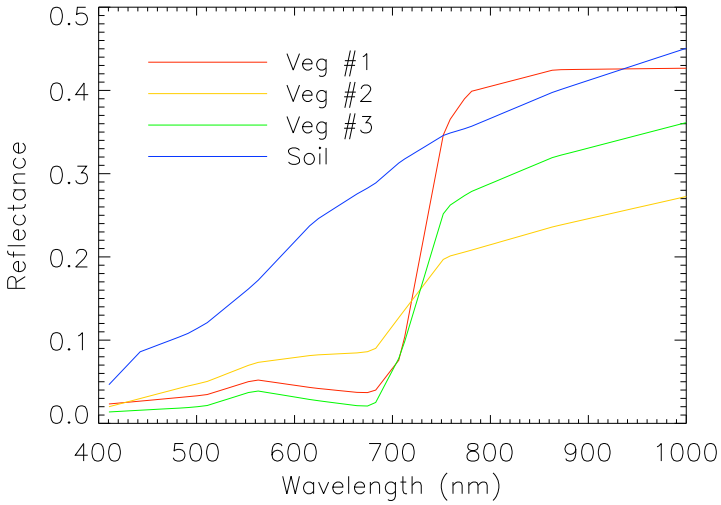

Figure 3: Vegetation and bare soil reflectance spectra used as endmembers in the aerosol retrieval module. The vegetation spectra correspond to a green vegetation crop (Veg #1), a typical forest spectrum (Veg #2) and a dark vegetation target (Veg #3).

reflectance has to be positive. The first band, centered in 410 nm, is avoided because of the high noise levels detected. The darkest pixel in the image is again used as a reference for the inversion.

2.1.4 Retrieval of columnar water vapor

Water vapor retrieval relies on a band-fitting approach making use of the water vapor absorption centered at 940 nm. The influence of the liquid water absorption in vegetation targets is minimised by discarding wavelengths longer than 930 nm, when the liquid water absorption becomes appreciable. This is illustrated in Fig. 4. An atmospheric total transmittance spectrum and typical green vegetation and bare soil spectra are plotted together. The NIR bands are separated into two regions, A and B, marked by grey bars. The first region, between 860 and 890 nm, is free from water vapor absorption, while the second one, between 890 and 930 nm, is affected by the left wing of the 940 nm absorption feature. However, the same linear response in the reflectance of land pixels is expected in the two regions. Thus, the surface reflectance in A can be derived by using climatology CWV values and extended to B by linear extrapolation. The resulting surface reflectance in AB is then independent of the water vapor influence, and can be used in the inversion of radiances in AB to estimate the CWV. A real band-fitting technique is only applied to modes 1 and 5, which are the ones providing a complete sampling of the 940 nm-water vapor absorption feature. In the case of the mode 3, only two bands, centered about 900 and 910 nm, are affected by that absorption. However, the inversion of these two bands following the procedure described before has shown to be sufficient for the accurate water vapor retrieval, as it will be discussed in the next section.

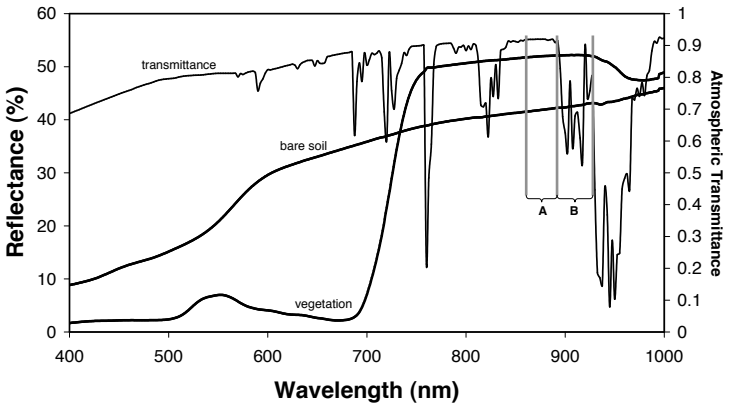

Figure 4: Green vegetation and bare soil reflectance spectra superposed to an atmospheric total transmittance spectrum. Labels "A" and "B" and grey bars mark the two spectral regions used in the CWV retrieval.

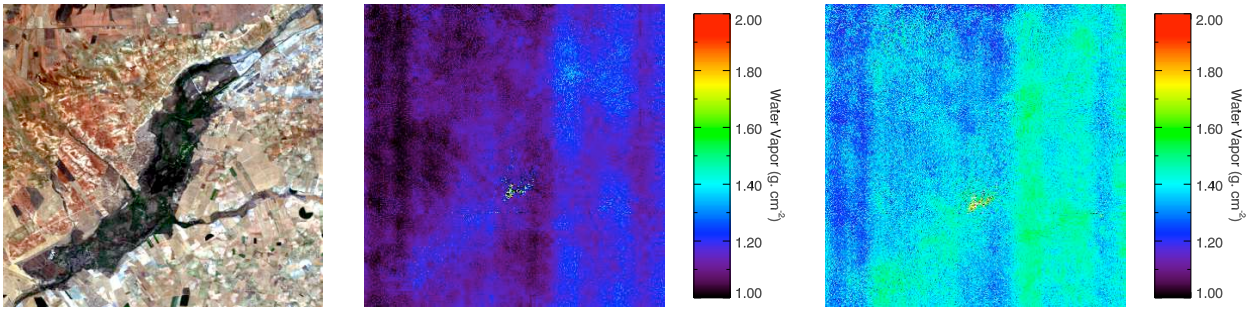

(a) RGB, 20 July 2007 (b) CWV, 20 July 2007 (c) CWV, 15 August 2007

Figure 5: CWV maps derived from CHRIS/PROBA images acquired over Las Tablas de Daimiel on two different dates.

The atmospheric parameters in the LUT are resampled to the sensor spectral configuration on a per-column basis, taking into account the spectral shift characterisation derived previously. The inversion of TOA radiance at AB regions spectral regiones is performed on a per-pixel basis so that the spatial distribution of CWV is derived. However, it must be admitted that CWV spatial distribution can be distorted to a large extent. The severe problems with vertical coherent noise in CHRIS/PROBA data makes some low-frequency striping patterns to be visible in CWV maps, even if the noise reduction module (Gómez-Chova et al., 2008a) has previously been applied to the data. As a result, CWV spatial patterns may be masked out by the impact of striping on CWV retrieval. A residual influence from surface reflectance can also be visible in the generated water vapor maps in most of the cases. An example of CWV maps derived from two different CHRIS/PROBA acquisitions over Las Tablas de Daimiel study site in summer 2007 is presented in Fig. 5. Mean and standard deviation CWV values are 1.13 ± 0.08 g·cm^{-2} for Fig. 5(b) and 1.38 ± 0.08 g·cm^{-2} for Fig. 5(c). Some water vapor structures can be noted even though they are superposed to both low-frequency striping and background influence.

In view of this fact, and taking into account that the per-pixel water vapor retrieval can be highly time consuming, an option for the code to perform water vapor ertrieval only on a selected subset of pixels, the retrieved mean value been applied to the complete image, can be selected by the user. This option is specially recommended in the case of flat, horizontally-homogeneous areas, where small variations in the spatial distribution of water vapor are expected.

2.1.5 Retrieval of surface reflectance

The derivation of the reflectance images is performed simultaneously to CWV retrieval, as the atmospheric parameters calculated for the inversion of CWV for each pixel can be used to invert Eq. 2.1 to obtain ρ_s. The spectral channel positions after the smile characterisation for modes 1 and 5 is already considered in the resampling of the corresponding atmospheric parameters.

Those initial reflectance images are refined by the removal of the image blurring caused by those photons reflected by the target environment and scattered by the atmosphere particles into the sensor's line-of-sight. This effect is called *adjacency effect*, because the apparent signal at the TOA for a given pixel comes also from the adjacent ones. The simple formulation proposed by Vermote et al. (1997) is followed here. It is based on the idea of weighting the strength of the adjacency effect by the ratio of diffuse to direct ground–to–sensor transmittance,

$$\rho'_s = \rho_s + \frac{t_d(\mu_v)}{e^{-\tau/\mu_v}}[\rho_s - \bar{\rho}], \tag{2.3}$$

where ρ'_s is the final surface reflectance, $t_d(\mu_v)$, $e^{-\tau/\mu_v}$ the transmittances for diffuse and direct radiation in the ground-to-sensor path, and $\bar{\rho}$ is the average of the environment reflectance.

The final step in the atmospheric correction scheme for modes 1 and 5 is the removal of systematic errors in surface reflectance. We refer to this step as "recalibration" or "spectral polishing". As systematic we consider the errors happening in surface reflectance with the same intensity and sign for all the targets. Out of absorption regions these errors are mostly due to problems in the instrument gain coefficients (radiometric calibration), but inside atmospheric absorptions they can also be associated to inaccurate radiative transfer simulations. The fact that they are systematic enables the correlation with an error-free reference reflectance for the correction. We assume that no errors are caused by dark current effects, but they are only due to problems in the gain coefficients.

The inversion of artificial endmembers is utilised again to provide the reference reflectance. The procedure works calculating equivalent smooth spectra by the inversion of the abundances $C_{v,s}$ in Eq. 2.2 against "spiky" spectra. Up to 50 reference spectra are extracted from the reflectance images derived using Eq. 2.1. The selection is made from a previous classification of the area based on three Normalized Difference Vegetation Index (NDVI) categories: vegetation, bare soil and mixtures. An equivalent smooth reflectance spectrum is calculated for each of the 50 reference spectra by inversion of $C_{v,s}$. A recalibration coefficient A_i for each channel is calculated then by correlating the 50 pairs of spectral reflectance from the spiky and smooth spectra. The reflectance image is finally multiplied by those coefficients to generate the final reflectance hypercube. Small

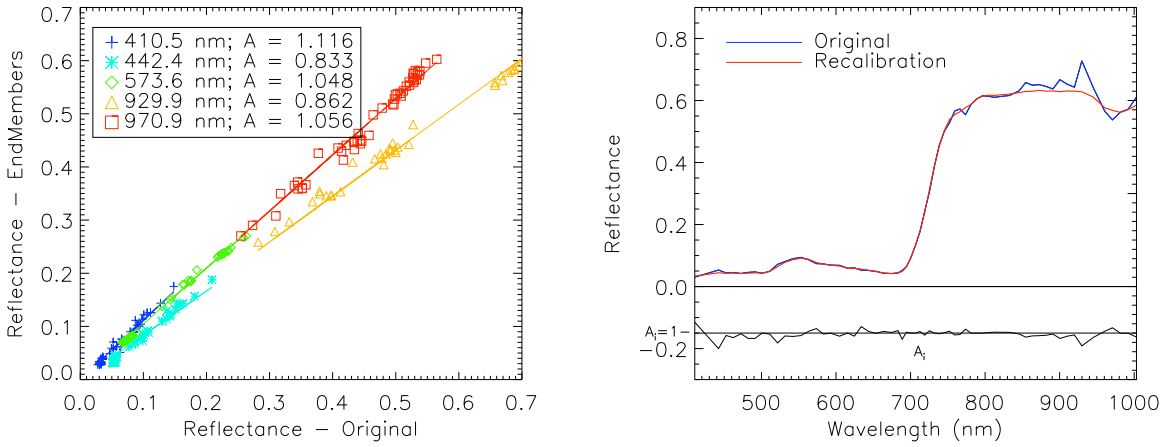

(a) (b)

Figure 6: Calculation of recalibration coefficients A_i. The correlation calculated for some channels is plotted in (a), and an example of "recalibrated" spectrum and the whole set of calibration coefficients is displayed in (b).

computation burden is performed thanks to the linearity of the problem, which allows linear regressions be used to calculate the endmember abundances. An example of the linear correlations calculated to derive the recalibration coefficients and a comparison between the original and the recalibrated data is shown in Fig. 6.

It must be remarked that this technique can lead to errors in reflectance for those images in which the endmembers can not reproduce the actual reflectance levels. For this reason, the recalibration process is carried out under user request and inspection.

2.2 Practical considerations

As it has already been discussed, the processing steps to be performed along the atmospheric correction process depend on the data acquisition mode. CHRIS acquisition modes 1 and 5 are the ones providing the best sampling of atmospheric absorption features in the visible and NIR region. The algorithm is implemented so that the processing can be performed automatically. The necessary inputs for the processing are read from the metadata attached to the original images. Those are view zenith and azimuth angle, site latitude and longitude, acquisition time and site mean elevation. Pixel quality masks and cloud probability images are provided by noise removal and cloud screening modules. Pixel-to-pixel elevation and topographic effects are not taken into account in the processing, as a digital elevation model (DEM) and the corresponding algorithm for its co-location with the images are not expected to be available. The mean elevation of the site is used instead for a first-order consideration of elevation-dependent effects. The neglection of pixel-to-pixel elevation changes could lead to noticeable errors for images acquired over rough terrain areas. Some other points to be remarked are:

- The assessment of spectral calibration and spectral polishing are only carried out over data acquired under modes 1 and 5.
- Band-fitting water vapor retrieval is performed on modes 1 and 5, while a retrieval algorithm based on the inversion of two spectral channels at the left wing of the 940 nm water vapor absorption feature is applied to mode 3 data. A climatology water vapor value is used for the processing of the other modes. This value can be changed by the user.
- AOT retrieval is performed automatically for the 5 acquisition modes. AOT can also be defined by the user if some a priori information from external data is available. An AOT value calculated by the aerosol optical depth retrieval module (Grey and North, 2007) can also be ingested by the algorithm. This would be recommended for arid or semi-arid environments, where no dark vegetation is available.
- Reflectance images and atmospheric AOT and CWV calculated as by-products are provided as outputs.
- The final step is the spectral polishing of the resulting reflectance data in modes 1 and 5. A comparison of initial and polished reflectance spectra is shown for 4 reference pixels during the processing. In view of those results, the user must confirm the application of the recalibration. This is the only interactive step along the processing.

According to the previous comments, there are some input parameters that can be changed by the user:

- `Cloud mask probability threshold:` It is the probability threshold to be applied to the probabilistic cloud mask for the discrimination between cloud-free and cloud-contaminated pixels. The default value is 0.05.
- `Aerosol Optical Thickness, 550 nm:` AOT at 550 nm which overrides the automatically-calculated value. It is recommended when ground-based aerosol measurements are available, or in arid or semi-arid regions where the AOT retrieval method is expected to fail. The aerosol optical depth retrieval module (Grey and North, 2007) can be used for the calculation of AOT in those cases.
- `Columnar Water Vapor Value:` Only in modes 2 and 4, water vapor value to be used for the processing of the complete image. A default season-dependent climatology value is used instead if this parameter is not provided.
- `Perform spectral polishing:` Only in modes 1 and 5, flag activating the final reflectance spectral polishing. The results from the polishing for 4 reference targets are displayed in the screen for user confirmation.
- `Perform derivation of water vapor map:` Only in modes 1, 3 and 5, flag activating the per-pixel water vapor retrieval procedure. By default, water vapor retrieval is only

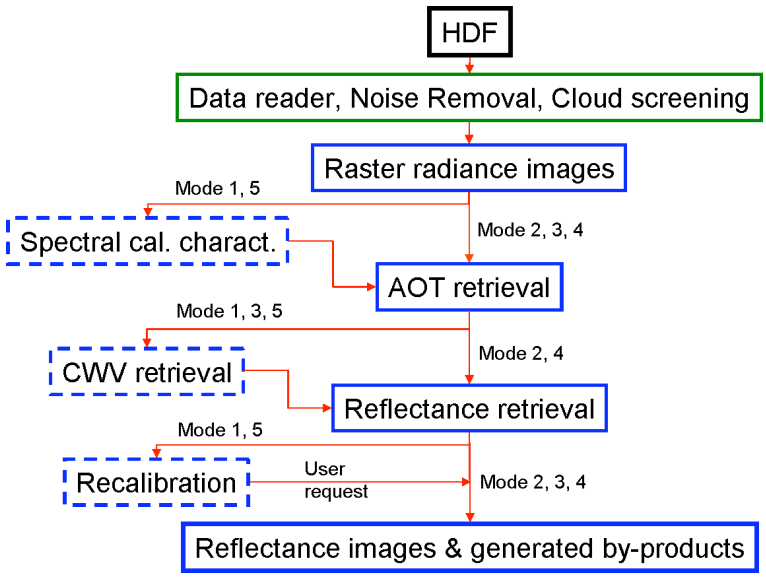

Figure 7: Flow chart describing the processing steps to be performed for the atmospheric correction of CHRIS/PROBA data, as a function of the acquisition mode.

performed over 50 land pixels. The mean water vapor value is applied for the processing of the complete image. The derivation of water vapor maps may results in total computation times of the order of 10 minutes per scene.

- `Perform Adjacency Correction:` Flag activating the adjacency correction described in Eq. 2.3. Adjacency is considered a second-order effect for low to medium aerosol loading, so the adjacency correction is not performed by default.

An schematic flow chart showing the processing steps to be performed in the conversion from the original images in `HDF` format to the final reflectance product is displayed in Fig. 7. The execution of noise removal and cloud screening modules prior to atmospheric correction is fully recommended.

3 Algorithm Validation

3.1 Reference ground-based data for validation

A useful data source for the validation of satellite-derived aerosol and water vapor parameters is the AErosol RObotic NETwork (AERONET) (Holben et al., 1998). AERONET is a network of stations measuring and archiving atmospheric parameters all over the world. Among other parameters, time-resolved spectral aerosol optical thickness and columnar water vapor are freely available at the AERONET web portal. AERONET stations located at CHRIS/PROBA acquisition sites and providing AOT and CWV data simultaneous to CHRIS/PROBA were identified. CHRIS/PROBA-derived AOT and CWV were compared with AERONET data from those stations. Up to 8 AERONET stations were found to be adequate for this validation exercise. Those

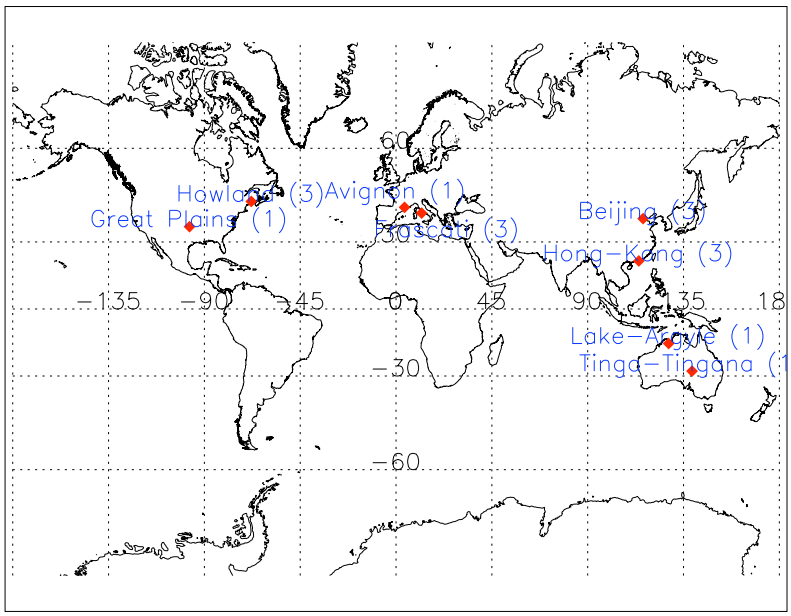

Figure 8: Location of the AERONET sites used in the validation of AOT and CWV retrievals from CHRIS/PROBA data. Numbers in brackets correspond to the mode of the CHRIS/PROBA acquisitions over each site.

are displayed in Fig. 8. Related CHRIS/PROBA sites correspond to either mode 1 or 3, as it is indicated by the numbers in brackets. Cloud-contaminated CHRIS/PROBA scenes were discarded by visual inspection. Three other AERONET stations around CHRIS/PROBA acquisition sites were found: Chibolton (51°N, 1°W), Solar Village (24°N, 46°E) and Mexico City (19°N, 99°W). No cloud-free images with simultaneuos AERONET measurements were found in the case of Chibolton, thin cirrus or fog contamination was present in most of the images from Mexico City, while Solar Village is located at a semi-desertic area without the minimum proportion of dark surfaces and spectral contrast required by the algorithm. An AOT value derived from the aerosol optical depth module or from existing climatology tables should be set in the input `Aerosol Optical Thickness` variable for this type of scenes.

On the other hand, ground-based reflectance measurements were available from some dedicated field campaigns. The SPectra bARrax Campaigns (SPARC) (Moreno, 2004) were held in the Barrax (39.05°N, 2.10°W, La Mancha, Spain) CHRIS/PROBA core site in July 2003 and 2004. The SENtinel-2 and FLuorescence EXperiment (SEN2FLEX) took place in June and July 2005. The Barrax site is a flat continental area with an average elevation over the sea level of around 700 m. There is a large contrast in natural surfaces, ranging from large homogeneous vegetation fields to large dry bare soils. The crops in the area were classified previously, so the comparison between in–situ surface reflectance measurements and the atmospherically corrected data is feasible for different land covers. Measurements of atmospheric parameters, such as AOT and CWV, were also carried out. Up to 9 CHRIS/PROBA data sets were acquired in summer

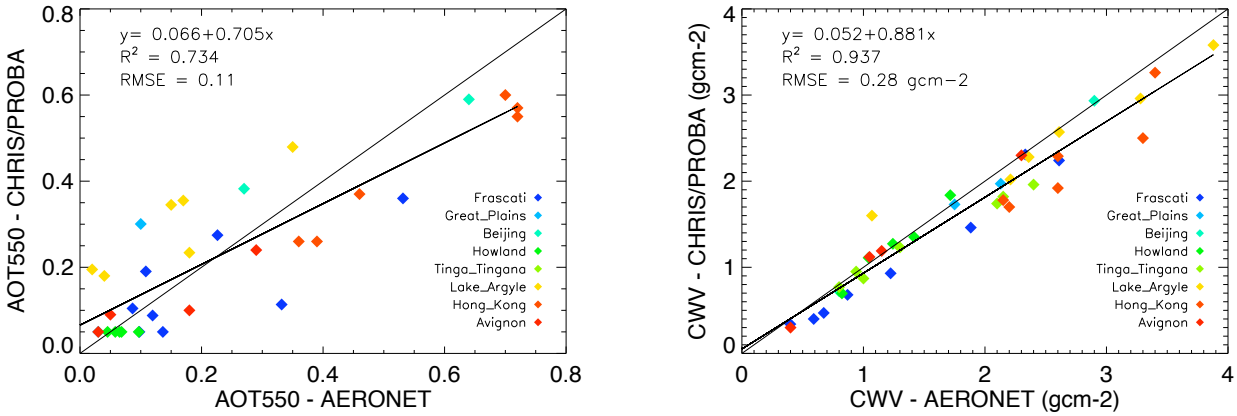

(a) (b)

Figure 9: Validation of CHRIS/PROBA-derived atmospheric parameters by comparison with AERONET data. Results from AOT at 550 nm are displayed in (a), while those from CWV are represented in (b).

2003, 2004 and 2005 over the Barrax area. All of them were acquired in mode 1.

3.2 Retrieval of atmospheric parameters

The comparison of CHRIS/PROBA AOT at 550 nm and CWV retrievals with AERONET data from the 8 stations mentioned before is displayed in Fig. 9. A relatively good correlation between CHRIS/PROBA and AERONET data is found for AOT retrievals, presented in Fig. 9(a), with a correlation coefficient R^2 of 0.734. It can also be noted that there is an underestimation in the retrieval of the highest AOT values. This is caused by the limitation of AOT at 550 nm to the range $0.05 - 0.6$ in the atmospheric LUT, as it was described in Table 1. Even though AOT at 550 nm values above 0.6 are only expected in very polluted urban areas (like Beijing or Hong-Kong in the plot), the extension of the LUT to higher aerosol loadings will be considered. The dependence of AOT retrieval on the particular site where the comparison is performed can also be noted. While good correlations at low and high aerosol loadings are calculated in Avignon and Hong-Kong, respectively, a systematic overestimation of CHRIS/PROBA with respect to AERONET is found in Lake Argyle. This can be explained by the bad performance of the method in semi-arid regions such as Lake Argyle.

The correlation between CHRIS/PROBA and AERONET data increases in the CWV case, as it is shown in Fig. 9(b). A wide range of CWV values from 0.3 to 4 g·cm^{-2} is registered. Even though some overestimation is also found for the largest CWV contents, a very high linear correlation of $R^2 = 0.937$ is calculated. Those can be reckon as satisfactory results, if one takes into account earlier problems of CHRIS/PROBA calibration at the NIR wavelengths which have been corrected by software (Cutter, 2004). No significative differences between sites is noted, despite the fact that both mode 1 and mode 3 data are combined in the comparison.

For further validation, the results from the *in-situ* atmospheric characterization performed

during the SPARC 2003 and 2004 campaigns (Martínez-Lozano et al., 2007) have been compared to CHRIS/PROBA results. The same exercise was already carried out with an older version of the algorithm (Guanter et al., 2005). Apart from a positive bias about 0.2 g·cm^{-2}, the good performance of CWV retrievals from CHRIS/PROBA data observed in the comparison with AERONET was confirmed for the 4 SPARC acquisition dates ($\{1.31, 1.62, 2.02, 2.13\}$ g·cm^{-2} from ground measurements, $\{1.58, 1.94, 1.83, 2.31\}$ g·cm^{-2} from CHRIS/PROBA). However, a worst correlation in AOT at 550 nm was found ($\{0.20, 0.28, 0.15, 0.24\}$ from ground measurements, $\{0.31, 0.19, 0.42, 0.26\}$ from CHRIS/PROBA) with respect to the old version of the algorithm. No solid explanation to this fact can be given, as the new models are based on a longer experience with CHRIS/PROBA data and other sensors, what led to more sophisticated approaches, and MODTRAN-based radiative transfer calculations have substituted the simpler 6S approach. It is expected that future tests at the same Barrax area can provide more information to be used for further algorithm improvement.

3.3 Retrieval of surface reflectance

3.3.1 Results from land targets

CHRIS/PROBA-derived surface reflectance is compared to ground-based measurements in Fig. 10. *In–situ* reflectance measurements were taken with an Analytical Spectral Devices (ASD) FieldSpec Pro FR Spectroradiometer (footprint around 0.8 m, 2 nm of spectral resolution). These measurements were acquired almost simultaneously to PROBA overpasses (time differences were always smaller than 30 minutes) from a nadir view while walking across the target, integrating in one spectrum all the measurements taken for every path of around 10 m. The reason for this procedure is to ensure that most of the natural variability in the target could be reproduced. The grey stripe in the plot gives the mean value and the standard deviation calculated from all the acquisitions made for the same target, in order to provide information on the spatial variability of the target.

The agreement between *in-situ* and CHRIS/PROBA data is relatively good, both in the shape and in the reflectance levels. It must be taken into account that the field spectra were acquired from a nadir view, not coincident with any of the PROBA view angles, so small deviations due to angular trends are expected a priori. This is confirmed by the fact that the maximum agreement with the in–situ measurements is found for the minimum view zenith angle angle. It can be stated that the comparison is especially good in the case of alfalfa and sunflowers targets. Large natural variations were found in the case of the sunflower crop, which consisted of plant rows separated by bare soil. The agreement reinforces the integrating procedure used in the ground measurements. For bare soils the directional effects are more important, what makes larger deviations are found in some targets. Finally, the bad comparison with the dry wheat crop might be explained by the practical difficulties in the measurement process, arisen because of the density and height of the plants.

Surface reflectance from the 5 view angles in 4 different targets are plotted in Fig. 11. An

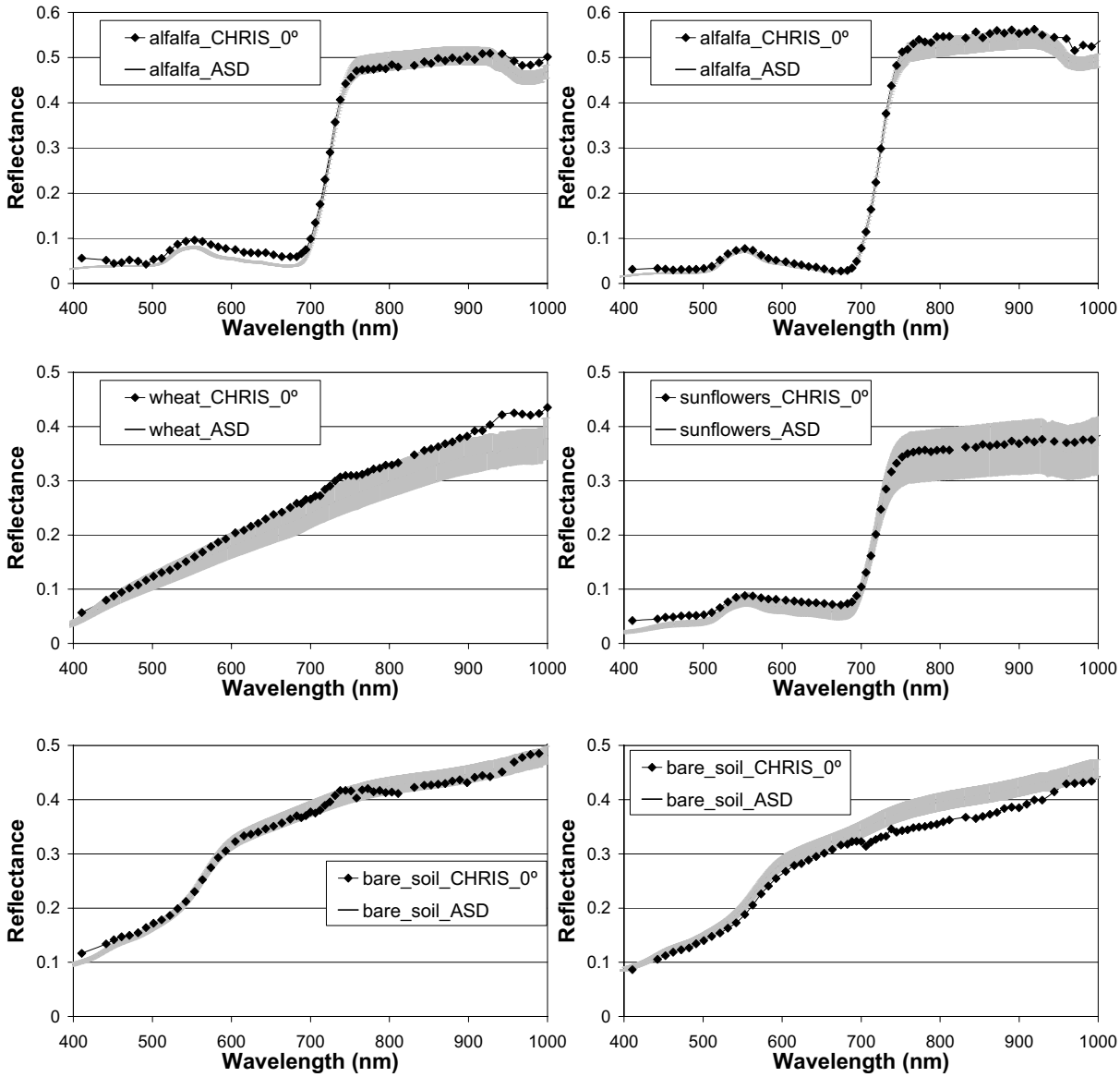

Figure 10: Sample surface reflectance spectra for different targets, compared with in–situ measurements taken with an ASD spectroradiometer. Plots in the left column come from SPARC 2003 data, and those in the right one from 2004.

accurate analysis of the directional effects appearing in those plots is out of the scope of this work, but some expected features can easily be noticed. It can be stated that the magnitude of the directional effects varies with the nature and vertical structure of the target as expected.

Since no in–situ multiangular measurements were available, the consistency of the directional behavior registered by the CHRIS/PROBA data has been checked using a coupled version of the SAIL and PROSPECT models (Miller et al., 2003) in order to simulate the reflectance of a real alfalfa crop. We have selected the alfalfa crop because of its 2–D uniformity, what makes it the prototype of crop to be modelled with the SAIL. Moreover, all the inputs needed (chlorophyll content, leaf area index, water content and dry matter content) were explicitly measured during

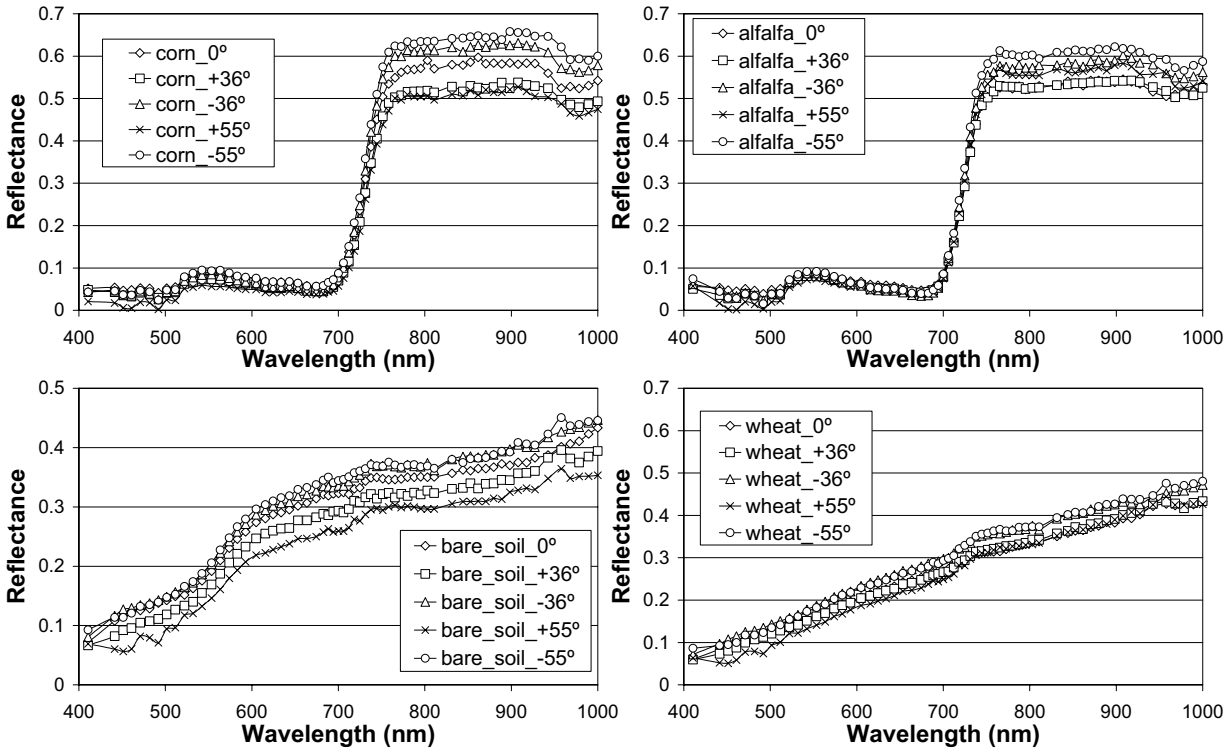

Figure 11: Composition of surface reflectance from different targets for the 5 different CHRIS/PROBA acquisition angles.

the SPARC 2004 campaign. Results for the 5 observation angles are plotted in Fig. 12. The input values for the model are shown in the legend. It can be stated that both the spectral shape (Fig. 12(a)) and the angular dependencies (Fig. 12(b)) are highly coincident with those showed for the alfalfa crop in Fig. 11, what confirms the validity of the procedure described in this work despite the Lambertian assumption, as well as the potential of CHRIS/PROBA to reproduce the reflectance trends of real surface, both in the spectral and angular domains.

3.3.2 Results from inland water targets

CHRIS/PROBA mode 2 images acquired over the Rosarito reservoir, located in Northern Spain (40.12°N, 5.27°W), were used to check the algorithm performance over inland water targets. Results obtained from the atmospheric correction of the image of 20 May 2004 are shown in Fig. 13. The 5 views of the same point in the Rosarito reservoir and the corresponding ground-based reflectance spectrum measured simultaneously to the CHRIS/PROBA acquisition are plotted. Ground-based measurements come from the Spanish Center for Hydrographic Studies (CEDEX), in the frame of its activities to validate algorithms for the monitoring of water quality using remote sensing data (Peña et al., 2004). A relatively high agreement between CHRIS data and the *in–situ* spectrum is found, taking into account the low signal arriving at the sensor from water targets and that the field measurement angle is not coincident with any of the CHRIS/PROBA

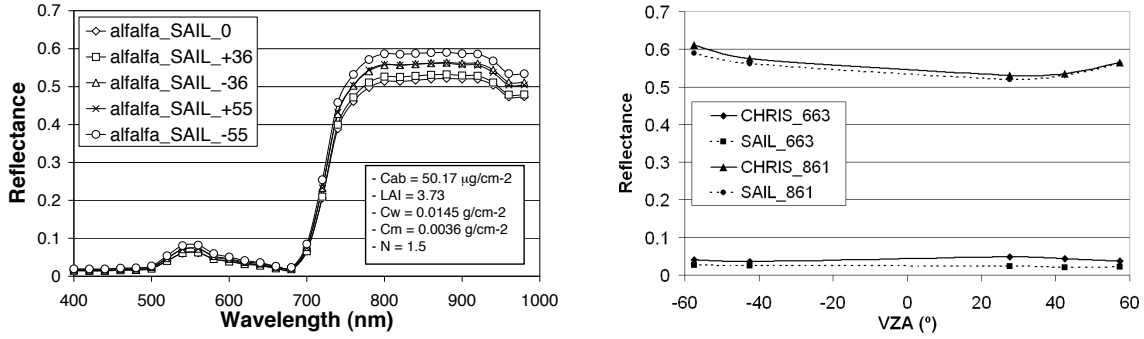

(a) (b)

Figure 12: Results of SAIL/PROSPECT simulations of alfalfa reflectance using *in–situ* measurements of biophysical parameters. The 5 reflectance spectra resulting from the simulations are plotted in (a), and the projection onto the 5 VZAs for 2 wavelengths in the red (663 nm) and in the NIR (861 nm) regions is plotted in (b).

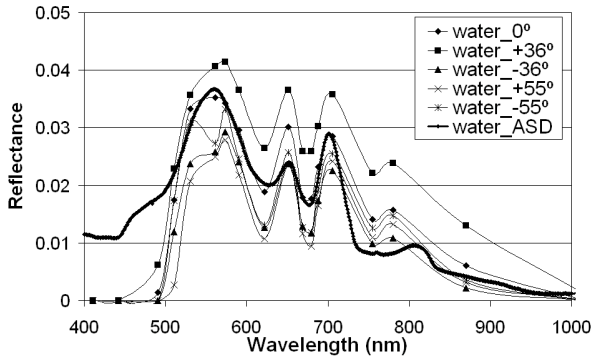

Figure 13: Comparison of CHRIS/PROBA-derived water reflectance spectra from the 5 observation angles with a spectrum acquired simultaneously *in-situ*.

observation angles. Nevertheless, the closest spectrum to the nadir–ASD measurement is again corresponding to the minimum VZA, as expected. This validates both the quality of CHRIS mode 2 data and the aerosol retrieval and atmospheric correction procedures implemented for inland water data.

4 Summary

The atmospheric correction algorithm for CHRIS/PROBA data to be implemented in the BEAM software has been described in this document. It is designed to process CHRIS/PROBA images in an automatic manner, independently of the CHRIS acquisition mode. The number of processing steps to be performed over the data are given by the spectral resolution and sampling of each mode. In the most general case, defined by modes 1 and 5, the entire atmospheric correction processing consists of characterisation of spectral calibration, AOT retrieval, CWV

retrieval, reflectance retrieval and data recalibration. Calibration assessment and CWV retrieval are not performed over modes 2, and 4 due to the insufficient sampling of atmospheric absorption features. This atmospheric correction module must follow noise reduction and cloud screening modules in the complete CHRIS/PROBA processing chain, even though cloud screening could be skipped when no cloud is observed in the image.

A general description of each processing step is provided in the first part of this document. Results from the application of previous versions of the algorithm to data acquired by the AERONET network or during specific validation campaigns are presented in the second part. Comparison with direct atmospheric measurements, ground-based reflectance measurements and modeled BRDF data show consistent results. Further validation through the processing of selected CHRIS/PROBA data representing the 5 acquisition modes and different environments and conditions is foreseen.

Acknowledgement

This work has been done in the frame of the project *Development of CHRIS/PROBA modules for the BEAM toolbox* (ESA ESRIN Contract No. 20442/07/I-LG). Previous algorithm developments were funded by the ESA–SPARC Project (ESA ESTEC–18307/04/NL/FF), the ESA–SEN2FLEX project (ESA ESRIN–19187/05/I-EC) and the DATASAT project (ESP2005-07724-C05-01, Ministry of Education and Science). The first author (LG) acknowledges the support by a PhD grant from the Spanish Government, Ministry of Education and Science. The authors also want to thank M. Cutter from Surrey Satellite Technology Ltd for his assistance with CHRIS technical issues, to R. Peña, J. A. Domínguez and A. Verdú from CEDEX for the provision with inland waters data, and to T. Schmidt, from CIEMAT, for Tablas de Daimiel data. The authors also want to thank the NASA and the Personal Investigators of all the AERONET stations providing data for this work.

Bibliography

Barnsley, M. J., Settle, J. J., Cutter, M., Lobb, D., and Teston, F. (2004). The PROBA/CHRIS mission: a low-cost smallsat for hyperspectral, multi-angle, observations of the earth surface and atmosphere. *IEEE Transactions on Geoscience and Remote Sensing*, 42:1512–1520.

Berk, A., Anderson, G. P., Acharya, P. K., Hoke, M. L., Chetwynd, J. H., Bernstein, L. S., Shettle, E. P., Matthew, M. W., and Adler-Golden, S. M. (2003). MODTRAN4 Version 3 Revision 1 User's Manual. Technical report, Air Force Research Laboratory, Hanscom Air Force Base, MA, USA.

Cutter, M. (2004). Review of aspects associated with the CHRIS calibration. In ESA/ESRIN, editor, *Proceedings of 2nd CHRIS/PROBA Workshop*, Frascati, Italy.

Fomferra, N. and Brockmann, C. (2005). BEAM - the ENVISAT MERIS and AATSR Toolbox. In ESA/ESRIN, editor, *Proceedings of the MERIS-(A)ATSR workshop*, Frascati, Italy.

Gómez-Chova, L., Alonso, L., Guanter, L., Calpe, J., and Moreno, J. (2008a). Algorithm Theoretical Basis Document for CHRIS/PROBA noise reduction. ESA ESRIN Contract No. 20442/07/I-LG.

Gómez-Chova, L., Guanter, L., Alonso, L., Calpe, J., and Moreno, J. (2008b). Algorithm Theoretical Basis Document for CHRIS/PROBA cloud screening. ESA ESRIN Contract No. 20442/07/I-LG.

Green, R. (1998). Spectral calibration requirement for earth–looking imaging spectrometers in the solar–reflected spectrum. *Applied Optics*, 37:683–690.

Grey, W. M. F. and North, P. R. J. (2007). PROBA/CHRIS Aerosol Optical Depth Retrieval Algorithm Theoretical Basis Document. ESA ESRIN Contract No. 20442/07/I-LG.

Guanter, L., Alonso, L., and Moreno, J. (2005). A method for the surface reflectance retrieval from PROBA/CHRIS data over land: Application to ESA SPARC campaigns. *IEEE Transactions on Geoscience and Remote Sensing*, 43:2908–2917.

Guanter, L., Richter, R., and Kaufmann, H. (2008). On the application of the MODTRAN4 atmospheric radiative transfer code to optical remote sensing. *International Journal of Remote Sensing*. In press.

Guanter, L., Richter, R., and Moreno, J. (2006). Spectral calibration of hyperspectral imagery using atmospheric absorption features. *Applied Optics*, 45:2360–2370.

Holben, B. N., Eck, T. F., Slutsker, I., Tanre, D., Buis, J. P., Setzer, A., Vermote, E., Reagan, J. A., Kaufman, Y., Nakajima, T., Lavenu, F., Jankowiak, I., and Smirnov, A. (1998). AERONET – a federated instrument network and data archive for aerosol characterization. *Remote Sensing of Environment*, 66:1–16.

Martínez-Lozano, J. A., Estellés, V., Molero, F., Gómez-Amo, J. L., Utrillas, M. P., Pujadas, M., Fortea, J. C., and Guanter, L. (2007). Atmospheric components determination from ground-level measurements during the Spectra Barax Campaigns (SPARC) field campaigns. *IEEE Transactions on Geoscience and Remote Sensing*, 45:2778–2793.

Miller, J. R., Berger, M., Alonso, L., Cerovic, Z., Goulas, Y., Jacquemoud, S., Louis, J., Mohammed, G., Moya, I., Pedros, R., Moreno, J. F., Verhoef, W., and Zarco-Tejada, P. J. (2003). Progress on the development of an integrated canopy fluorescence model. In *Proceedings of IGARSS*, Toulouse (France).

Moreno, J. (2004). The SPECTRA Barrax Campaign (SPARC): Overview and first results from CHRIS data. In ESA/ESRIN, editor, *Proceedings of 2nd CHRIS/PROBA Workshop*, Frascati, Italy.

Mouroulis, P., Green, R. O., and Chrien, T. G. (2000). Design of pushbroom imaging spectrometers for optimum recovery of spectroscopic and spatial information. *Applied Optics*, 39:2210–2220.

Nicodemus, F. E., Richmond, J. C., Hsia, J. J., Ginsberg, I. W., and Limperis, T. (1977). Geometrical considerations and nomenclature for reflectance. Technical report, National Bureau of Standards, US Department of Commerce, Washington, DC, USA.

Peña, R., Ruiz, A., and Domínguez, J. A. (2004). CEDEX proposal for CHRIS/PROBA activities in 2004 on validation of MERIS models. In *Proceedings of CHRIS/Proba Workshop*, ESA–ESRIN, Frascati (Italy).

Press, W. H., Flannery, B. P., Teukolosky, S. A., and Vetterling, W. T. (1986). *Numerical Recipes*. Cambridge University Press.

Qu, Z., Kindel, B. C., and Goetz, A. F. H. (2003). The High Accuracy Atmospheric Correction for Hyperspectral Data (HATCH) Model. *IEEE Transactions on Geoscience and Remote Sensing*, 41:1223–1231.

Vermote, E. F., El-Saleous, N., Justice, C. O., Kaufman, Y. J., Privette, J. L., Remer, L., Roger, J. C., and Tanré, D. (1997). Atmospheric correction of visible to middle infrared EOS-MODIS data over land surface: Background, operational algorithm and validation. *Journal of Geophysical Research*, 102:17131–17141.

von Hoyningen-Huene, W., Freitag, M., and Burrows, J. P. (2003). Retrieval of aerosol optical thickness over land surfaces from top-of-atmosphere radiance. *Journal of Geophysical Research*, 108:4260–4279.